Understanding exotic black hole orbits using effective potentials

Steven Pakiela, Brett Bolen,[a] and Benjamin P. Holder[b]
Department of Physics, Grand Valley State University, Allendale, Michigan 49504

Monica Rizzo and Shane L. Larson[c]
Center for Interdisciplinary Exploration and Research in Astrophysics, Northwestern University, Evanston, Illinois 60208

(Received 7 March 2023; accepted 21 June 2024)

Strongly gravitating systems can undergo unusual orbital trajectories. For example, "extreme mass ratio inspirals" (observable in the megahertz band by space-based gravitational wave detectors) can exhibit "zoom-whirl" orbits, which make complicated waveforms that are useful for mapping out the system's gravitational structure. Zoom-whirl behavior can be intuitively understood in the context of effective potentials, which should be familiar to students from classical orbital theory in mechanics. Here, we explore zoom-whirl orbits using effective potential theory around Schwarzschild black holes and present an interactive tool that can be used in pedagogical settings.
© *2024 Published under an exclusive license by American Association of Physics Teachers.*
https://doi.org/10.1119/5.0149655

I. INTRODUCTION

Traditional training in physics develops core paradigms that underpin much of the discipline and are pedagogically quite useful.[1] Such paradigms are not only useful for solving textbook problems, but also for understanding complex and exotic behavior in physical systems. This paper illustrates how effective potentials, typically introduced to students in the context of classical mechanics and scattering theory, can be utilized in gravitational wave astronomy to understand "zoom-whirl" orbits. These orbits are expected to be common in extreme-mass-ratio-inspirals (EMRIs) of small compact objects into supermassive black holes;[2] the EMRI name was coined by Glampedakis and Kennefick in 2002.[3] Zoom-whirl orbits have been actively studied over the past 20 years[3–9] and will be a key source for the Laser Interferometer Space Antenna (LISA), expected to launch in the mid-2030s.[4,10,11] When visualized, these orbits appear random and unpredictable, but studies have shown their behavior is not formally chaotic.[12] EMRIs are valuable observational sources, in part because zoom-whirl trajectories traverse much of the volume around the central massive object. If such orbits can be reconstructed from their gravitational wave signals, they provide a detailed map of the spacetime around the black hole. This is completely analogous to *geodesy*, the careful mapping of the gravitational environment of the Earth from observations of satellite trajectories.

As is common in general relativity, throughout the paper we use geometrized units $G = c = 1$,[13,14] where G is the gravitational constant and c is the speed of light.[15] To restore G and c to any equation, multiply each quantity in the equation by a conversion factor:[14] if the quantity has dimension length$^l \times$ time$^m \times$ mass^n, it should be multiplied by a factor of $c^m(G/c^2)^n$.

This paper is organized as follows: In Sec. II, we review the basics of EMRIs and zoom-whirl orbits. Section III A provides the effective potential framework for orbits around a Schwarzschild black hole, while Secs. III B and III C apply the effective potential theory to illustrate how zoom-whirl orbits arise and analytically determine the number of whirls. Then, in Sec. IV, we provide a brief overview of both the production and detection of gravitational radiation. Section V discusses an online visualization tool we developed. The codes underlying this tool are publicly available on GitHub,[16] and the simulation tool itself can be used to output plots and datasets like those displayed in this work. Finally, in Sec. VI, we summarize our results and discuss the utility of the theory and simulation tools for the undergraduate classroom.

II. EXTREME MASS RATIO INSPIRALS

Newtonian gravity provides reasonable accuracy for most calculations of solar system dynamics. However, precision measurements, such as the observations of Mercury's perihelion precession, reveal that Newtonian gravity is simply the weak field limit of the underlying theory of general relativity. Bertrand's theorem states that the inverse square law and Hooke's law are the only central force laws that give rise to closed orbits for all bound particles. As will be shown in Sec. III, relativistic effects can be captured rigorously by using an effective potential, which, according to Bertrand's theorem, cannot possess closed orbits.[17] Thus, orbits in Einstein's theory of general relativity, even for planets in the solar system, cannot be closed.

In the context of zoom-whirl orbits in extreme mass ratio systems, the consequences of Bertrand's theorem are even more dramatic. Compact stellar remnants, such as neutron stars or black holes of mass $\sim 10\,M_\odot$, are expected to be captured by massive black holes of mass $\gtrsim 10^6\,M_\odot$ in the centers of galaxies.[18] These orbits are expected to be highly eccentric, where the light companion "zooms" outward to a large radius before making a close encounter with the central black hole. The perihelion of the orbit will precess during the close encounter; under certain conditions, this precession can be extreme, resulting in a "whirl" where the companion makes many loops around the central mass before zooming out to large radii again. Over time, the system loses energy to gravitational radiation, causing the orbit to shrink and become more and more circular until the compact body plunges into the central black hole.

In astrophysical contexts, these central black holes are expected to rotate and can be represented by the Kerr

06 December 2024 17:35:28

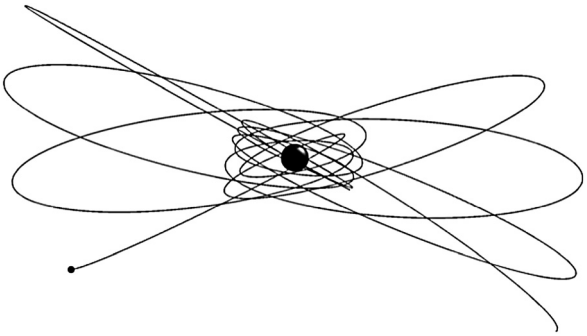

Fig. 1. A classic zoom-whirl trajectory generated by a three-dimensional simulation of an object orbiting around a spinning black hole.[19]

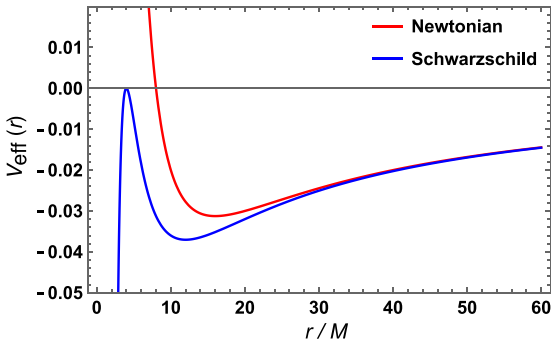

Fig. 2. A comparison of the Newtonian effective potential and the Schwarzschild effective potential for $\tilde{\ell} = 4M$. Note how the additional $1/r^3$ term in the Schwarzschild case dominates at small radii, creating a local maximum.

solution to Einstein's equations. A three-dimensional simulation of a zoom-whirl trajectory around a spinning (Kerr) black hole is shown in Fig. 1. As we show here, this behavior is actually not a consequence of the spin of the black hole; instead, the zoom-whirl behavior is a feature of the effective potential experienced by the orbiting object, and can occur even if the central massive object is not rotating. To that end, we will derive the zoom-whirl behavior from the equations of motion for a test particle in the effective potential of a stationary Schwarzschild (spherical, non-spinning) black hole.

III. EFFECTIVE POTENTIALS

A. Comparison of Newtonian and Schwarzschild effective potentials

From classical mechanics, the equation of motion of a particle (with mass m) in orbit around a massive body (with mass M) has the following form:

$$m\ddot{r} = -\frac{\mathrm{d}}{\mathrm{d}r}\left(V(r) + \frac{\ell^2}{2mr^2}\right) \tag{1}$$

(over-dots represent time derivatives). Here, $\ell = mr^2\dot{\phi}$ is the angular momentum, a constant of the motion; the energy $(E = 1/2\, m\dot{r}^2 + V(r) + \ell^2/2mr^2)$ is also a conserved quantity. The term inside the parentheses in Eq. (1) is called the "effective potential." In Newtonian gravity, $V(r) = -Mm/r$; dividing both sides of Eq. (1) by the mass of the orbiting particle and defining $\tilde{\ell} = \ell/m$, $\tilde{E} = E/m$, and $\tilde{V} = V/m$, we have $\ddot{r} = -d\tilde{V}_{\rm eff,Newt}(r)/dr$, which defines the *specific* Newtonian effective potential,

$$\tilde{V}_{\rm eff,\,Newt}(r) = -\frac{M}{r} + \frac{\tilde{\ell}^2}{2r^2}. \tag{2}$$

In general relativity, one can derive an equation of motion for a particle moving in the spacetime around a Schwarzschild black hole and cast it in the same language of effective potentials $\ddot{r} = -d\tilde{V}_{\rm eff,Schd}(r)/dr$. Energy and angular momentum are again conserved, but the specific effective potential has an additional term,[20]

$$\tilde{V}_{\rm eff,Schd} = -\frac{M}{r} + \frac{\tilde{\ell}^2}{2r^2} - \frac{M\tilde{\ell}^2}{r^3} = -\frac{M}{r} + \frac{\tilde{\ell}^2}{2r^2}\left(1 - \frac{R_s}{r}\right), \tag{3}$$

where $R_s = 2M$ is the Schwarzschild radius. The third term scales like $1/r^3$; it is negligible at large radii, leading to near-Newtonian behavior far from the black hole, but it dominates at small radii near the central black hole. The additional relativistic term creates a second extremum in the potential, with a local maximum near the black hole (but outside the event horizon at R_s). Henceforth, we will suppress the identifying subscript on the effective potential, and $V_{\rm eff}$ will mean the Schwarzschild effective potential. Both the Newtonian and general relativistic potentials are illustrated in Fig. 2.

The effective potential is useful for classifying types of orbits: intersections of the constant orbital energy, $\tilde{E}$, with the effective potential indicate orbital turning points, where $\dot{r} = 0$ (in the general relativistic situation, time derivatives are taken with respect to proper time, τ). In the Schwarzschild case, however, the types of allowable orbits depend on the value of the angular momentum. The situation for $\tilde{\ell} > 4M$ is shown schematically in Fig. 3. A stable *circular* orbit exists for $\tilde{E}$ equal to the local minimum of the potential (similarly, there is an unstable circular orbit for $\tilde{E}$ equal to the potential's local maximum). *Bound* orbits ($\tilde{E} < 0$) have an inner turning point (periapsis, r_p) and an outer turning point (apoapsis, r_a). When the particle energy is exactly zero, the orbit is *parabolic*. When $\tilde{E} > 0$, the orbit can be *unbound* (hyperbolic) or *plunging* ($\tilde{E} > \max[V_{\rm eff}]$). For angular momentum values $\sqrt{12}M < \tilde{\ell} < 4M$, the local maximum of the effective potential is below zero and no unbound orbits are allowed. For $\tilde{\ell} < \sqrt{12}M$, the potential has no inner peak and thus no bound orbits.*

B. Whirling in effective potentials

The whirling behavior prevalent in EMRIs can be understood as a very strongly precessing orbit. To help build intuition for this extreme case, it helps to first examine a more familiar example from the solar system. The famous "anomalous" perihelion advancement observed in Mercury's orbit cannot be explained by Newtonian gravity—explaining this advance was one of the first proofs of Einstein's theory[21]—and it can be understood by comparing the Newtonian and Schwarzschild effective potentials.

To see the origin of periapsis precession from the effective potential, first note that the angular speed ($u^\phi = \dot{\phi}$, the azimuthal component of the four-velocity) is

*The condition $\tilde{\ell} \geq \sqrt{12}M$ for which the effective potential can support bound orbits is found by requiring real solutions to $\mathrm{d}V_{\rm eff}/\mathrm{d}r = 0$.

06 December 2024 17:35:28

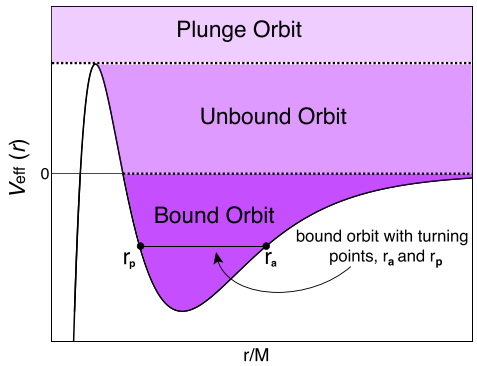

Fig. 3. A schematic of the effective potential for a particle around a Schwarzschild black hole with $\tilde{\ell} > 4M$, showing the energy regimes for various orbits: circular (where $dV_{\rm eff}/dr = 0$), bound ($\tilde{E} < 0$), parabolic ($\tilde{E} = 0$), unbound ($0 < \tilde{E} < \max[V_{\rm eff}]$), and plunging ($\tilde{E} > \max[V_{\rm eff}]$). If $\tilde{\ell}$ were below $4M$, the local maximum of the effective potential would be below zero, eliminating the region of unbound orbits. The horizontal axis is in the log scale to show the full potential well.

$$u^{\phi} = \frac{\tilde{\ell}}{r^2}, \tag{4}$$

therefore, as r becomes smaller, u^{ϕ} increases in accordance with the conservation of angular momentum. As shown in Fig. 2, the inner turning point in the Schwarzschild potential is *always* at a smaller radius than that in the Newtonian potential, meaning a higher angular speed as the particle approaches the turning point, and the accumulation of more orbital phase, resulting in the "anomalous advance" in the periapsis on the next orbit.

The whirling behavior in extreme mass ratio systems can also be understood from the unique shape of the Schwarzschild effective potential. The radial kinetic energy is the difference between the energy of the orbit, $\tilde{E}$, and the effective potential, $\tilde{V}_{\rm eff}$. Thus, $\dot{r}$ changes rapidly when $\tilde{V}_{\rm eff}$ changes rapidly, and $\dot{r}$ changes slowly when $\tilde{V}_{\rm eff}$ changes slowly. As the particle approaches an orbital turning point, $\dot{r} \to 0$.

Consider an orbiting particle whose energy $\tilde{E}$ is only slightly less than the Schwarzschild effective potential energy at its local maximum (Fig. 4), such that the inner turning point is very near the extremum of the potential. When the particle is very close to the turning point, its radial speed $\dot{r}$ is very small but changing (relatively) slowly because the slope of the potential is shallow. Since the radius is approximately constant during the extended time the particle is in this region of the potential, u^{ϕ} is approximately constant and the phase $\Delta\phi$ is rapidly accumulating—the particle is "whirling." Eventually, the particle reaches its turning point, $\dot{r} = 0$, and begins moving toward larger radii; u^{ϕ} begins to decreases, and the accumulation of phase slows. The whirling phase ends as the zoom phase of the orbit commences again. The rapid precession of the whirling phase is closely connected to the presence of a local maximum in the potential.

C. Explicit calculation of whirliness

Conventionally, a complete orbital period is defined as the time required to travel from periapsis to periapsis. For a Newtonian orbit, the particle traverses an angle of $\phi = 2\pi$ during that period. However, for fast-precessing orbits, the

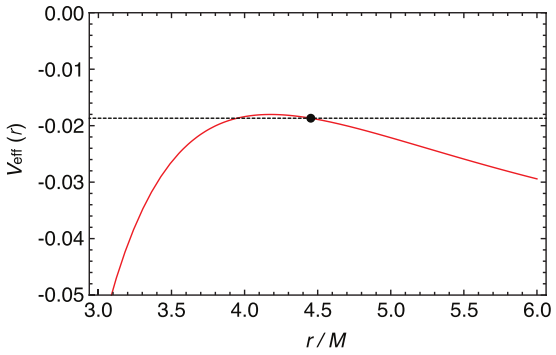

Fig. 4. Magnified view near the local maximum of the effective potential with $\tilde{\ell} = 3.85\,M$. The inner turning point of the orbiting particle (dot) occurs where its orbital energy ($\tilde{E} = -0.0185$, dashed line) intersects the effective potential.

advance in ϕ can be more than 2π in the time between two successive periapse passes.

Periapsis precession is most often reported as a rate of change in the angular position; for instance, Mercury's perihelion advance is 574 arcseconds/century. In the case of zoom-whirl orbits, however, the precession is enormous in a very short time—"whirling" refers to multiple circuits of the black hole per periapsis approach—so it is more convenient to define the "whirliness" of the orbit as

$$\varpi = \frac{\Delta\phi}{2\pi}, \tag{5}$$

where $\Delta\phi$ is the total accumulated angular phase between successive periapsis passes, as viewed by an observer far from the black hole. The normalization factor of 2π is the expected accumulated phase in a Keplerian (closed) orbit, and such an orbit has a whirliness $\varpi = 1$. The whirliness associated with objects in the solar system is a miniscule correction to Kepler; for example, Mercury's precession corresponds to $\varpi \approx 1 + 10^{-6}$. For strongly precessing zoom-whirl orbits, one can view the whirliness ϖ as the number of loops the particle makes around the black hole in one periapsis to periapsis cycle (according to a distant observer).

The computation of the whirliness ϖ is most easily accomplished by writing out the components of the particle 4-velocity, u^{α},

$$u^{r} = \dot{r} = \sqrt{2\tilde{E} - \frac{\tilde{\ell}^2}{r^2} + \frac{2M}{r}} \tag{6}$$

and

$$u^{\phi} = \frac{\tilde{\ell}}{r^2}. \tag{7}$$

These equations can be used to either numerically evaluate the whirliness, or to construct a mathematical transformation that allows ϖ to be written in closed form.

A useful analytic form of the whirliness can be found by re-expressing $\dot{r}$ and $\dot{\phi}$ in terms of new auxiliary parameters: the relativistic eccentricity and relativistic semi-latus rectum. This is a classic method appearing in the literature,[2,22,23] and a modern textbook implementation with extended discussion can be found in Ref. 24, which we follow here. Nonrelativistically, an ellipse's semi-latus rectum is half the length of the chord, which passes through a focus and is

06 December 2024 17:35:28

perpendicular to the major axis. For a fast-precessing orbit, the relativistic counterparts of the semi-latus rectum and the eccentricity are less straightforward to visualize geometrically, but they are defined naturally in terms of periapsis, r_p, and apoapsis, r_a. The relativistic semi-major axis is defined as $a = (r_p + r_a)/2$, while the relativistic semi-latus rectum, p, and the relativistic eccentricity, e, are together defined by

$$r_p = \frac{p}{1+e}, \quad r_a = \frac{p}{1-e}, \tag{8}$$

where the relativistic eccentricity is $e = 0$ for a circular orbit and $0 < e < 1$ for a bound orbit, completely analogous to the Keplerian case. Note that the above-mentioned expressions imply that $p = a(1-e^2)$.

Assuming a bound orbit, and using Eq. (3) for the effective potential, the cubic equation $\tilde{E} - \tilde{V}_{\text{eff, Schd}} = 0$ can be factorized as $k(1/r - 1/r_0)(1/r - 1/r_a)(1/r - 1/r_p) = 0$, where k is a constant and r_0 is the innermost crossing of the potential function, where it is descending. Using Eq. (8), this allows one to write the specific angular momentum and specific energy as[24]

$$\tilde{\ell}^2 = \frac{Mp}{1 - \frac{1}{2}(3+e^2)R_s/p}, \tag{9}$$

$$\tilde{E} = -\frac{M}{2p}(1-e^2)\left(\frac{1-2R_s/p}{1-\frac{1}{2}(3+e^2)R_s/p}\right), \tag{10}$$

where $R_s = 2M$ is the Schwarzschild radius. Note that when the semi-latus rectum is much larger than a Schwarzschild radius ($p \gg R_s$), these equations give the Newtonian limit for elliptical orbits $\tilde{\ell} = \sqrt{Mp}$ and $\tilde{E} = -(M/2p)(1-e^2)$.

To derive a closed form expression for the whirliness, ϖ, it is convenient to parameterize the orbit in terms of an angular parameter χ, rather than the conventional azimuthal angle ϕ. This parameter has the value $\chi = 0$ at periapsis and $\chi = \pi$ at apoapsis; it is related to ϕ for circular orbits by

$$\phi = \frac{1}{\sqrt{1 - 3R_s/p}}\chi. \tag{11}$$

This parameterization is convenient because it accounts for the curvature of space near the black hole horizon. For noncircular orbits at semi-latus rectum values far from the horizon, $\chi \approx \phi$, giving the classic Keplerian result. For general orbits, the relation between ϕ and χ can be found by starting with the shape equation of the orbit,

$$r(\chi) = \frac{p}{1 + e\cos(\chi)}. \tag{12}$$

As expected, far from the black hole, where $\chi \approx \phi$, this gives the shape equation in Newtonian gravity, $r(\phi) = p/(1 + e\cos\phi)$. The whirliness can be evaluated by finding $\mathrm{d}\phi/\mathrm{d}\chi$,

$$\Delta\phi = \int d\phi = \int_0^{2\pi} \frac{\mathrm{d}\phi}{\mathrm{d}\chi}\mathrm{d}\chi. \tag{13}$$

Using the definitions of $\tilde{\ell}$ and $\tilde{E}$, the difference between the specific total mechanical energy and the specific potential energy is

$$\tilde{E} - \tilde{V}_{\text{eff}} = \frac{M}{2p}e^2\sin^2\chi\left(\frac{1-(3+e\cos\chi)R_s/p}{1-\frac{1}{2}(3+e^2)R_s/p}\right). \tag{14}$$

From energy conservation, the total specific mechanical energy is

$$\frac{1}{2}\dot{r}^2 + \tilde{V}_{\text{eff}} = \tilde{E}. \tag{15}$$

Solving this for $\dot{r} = dr/d\tau = \sqrt{2(\tilde{E} - \tilde{V}_{\text{eff}})}$ and using Eqs. (4), (9), (12), and (14), yields

$$\frac{\mathrm{d}\phi}{\mathrm{d}\chi} = \frac{d\phi}{d\tau}\frac{d\tau}{dr}\frac{dr}{d\chi} = \frac{1}{\sqrt{1-(3+e\cos\chi)R_s/p}}. \tag{16}$$

Substituting Eq. (16) in Eq. (13) allows for the computation of the whirliness. The results are shown in Fig. 5. In the Newtonian limit, we can Taylor expand in the small parameter R_s/p to get

$$\Delta\phi = 2\pi + 6\pi\left(\frac{R_s}{p}\right) + \frac{3\pi}{2}(18+e^2)\left(\frac{R_s}{p}\right)^2 + \cdots. \tag{17}$$

Here, the leading term is the Keplerian result, and the difference between the leading term and the first order term is the classic periapsis shift term for Schwarzschild.

We have discussed whirliness in the context of noncircular orbits. However, examination of Eq. (17) shows that the higher order terms in the expansion do not tend to zero when the orbit becomes circular. What does it mean to have a periapsis shift for a circular orbit? This is a question about an effect that is not observable, since there is no fixed reference point to identify the periapsis of the circular orbit.

IV. GRAVITATIONAL WAVES

There is great interest in zoom-whirl orbits around massive black holes because these are prospective sources for

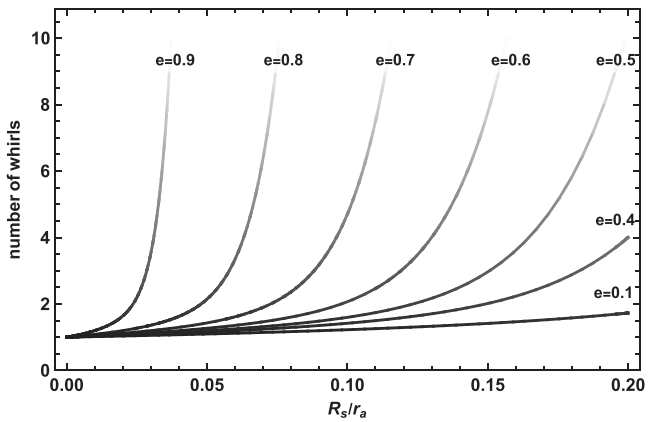

Fig. 5. The "whirliness" of an orbit—the angular distance a particle travels from periapsis to periapsis, divided by 2π—as a function of the ratio of the Schwarzschild radius to the apoapsis r_a (rightward is the direction of increasing apoapsis), for various values of the eccentricity. Note that there are two factors that govern how an orbit's angular distance deviates from that of a Newtonian closed orbit. First, as eccentricity increases, the orbit's apoapsis more closely approaches the local maximum of the effective potential. Second, the whirliness is strongly affected by how closely r_a approaches the Schwarzschild radius.

06 December 2024 17:35:28

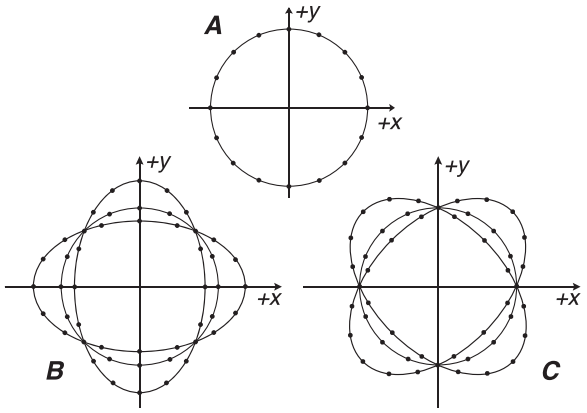

Fig. 6. A circular ring of test particles in the x-y plane (panel A). The proper distance between particles in the ring is distorted, elongated along one axis and compressed along the orthogonal axis, oscillating as a gravitational wave propagates perpendicular to the plane of the ring. The dynamics are shown for a + polarized wave (panel B) and a × polarized wave (panel C).

low-frequency gravitational wave observatories like LISA. In the limit presented here, for a static background potential and particle trajectories that are geodesic, it is straightforward to compute the gravitational waveforms generated by these orbits.

The gravitational wave amplitude h^{TT}_{jk} at time t and at a distance d from the source can be found using the quadrupole formula first derived by Einstein,[25,26]

$$h^{\mathrm{TT}}_{jk}(t,d) = \frac{2}{d}\ddot{\mathcal{I}}^{\mathrm{TT}}_{jk}(t-d), \tag{18}$$

where $t-d$ is the time of emission and where

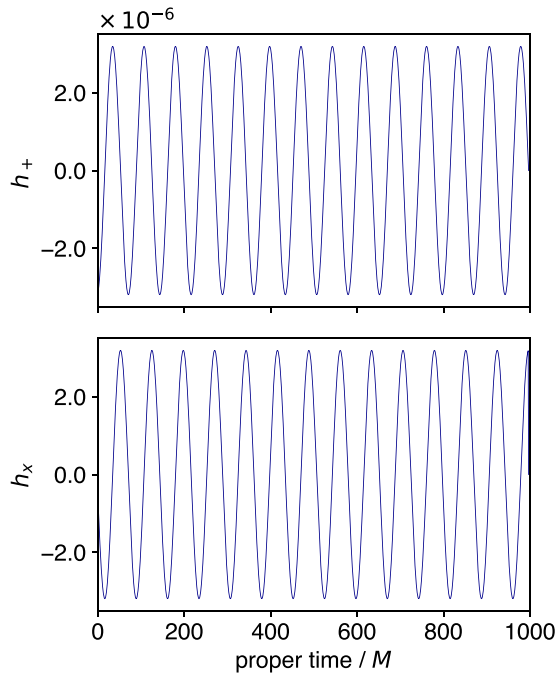

Fig. 7. The + (top panel) and × (bottom panel) waveforms for a circular ($e=0.0$) orbit ($\tilde{\ell}/M = 3.7$ and $\tilde{E} = -4.541 \times 10^{-2}$). In this and the following figures, the data were exported directly from the online dashboard,[16] assuming that the mass ratio of the orbiting particle to the central black hole was $m/M = 10^{-5}$.

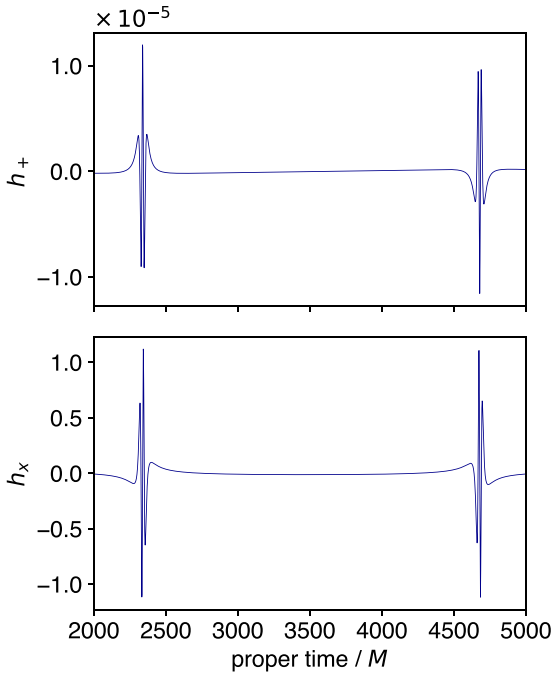

Fig. 8. The + (top panel) and × (bottom panel) waveforms for an eccentric ($e=0.9$) orbit ($\tilde{\ell}/M = 3.98$ and $\tilde{E} = -9.70 \times 10^{-3}$).

$$\mathcal{I}^{\mathrm{TT}}_{jk}(t) = \int \rho(t,\vec{x})\left[x_j x_k - \frac{1}{3}|\vec{x}|^2\delta_{jk}\right]d^3x \tag{19}$$

is the *transverse traceless quadrupole moment tensor*, which is related to the familiar moment of inertia tensor in classical mechanics that characterizes the distribution of mass in a system. Note: h^{TT}_{jk} is dimensionless, so to restore non-

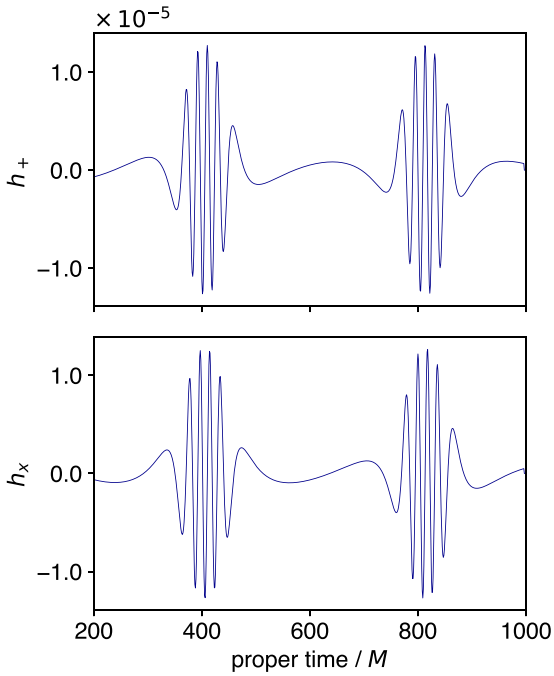

Fig. 9. The + (top panel) and × (bottom panel) for an orbit with orbital energy near the peak of the effective potential ($\tilde{\ell}/M = 3.7$, $\tilde{E} = -3.445 \times 10^{-2}$). The waveform clearly shows many oscillating peaks during the whirling phase, separated by a slowly-changing, low-amplitude regime during the zoom phase.

06 December 2024 17:35:28

geometrized units to Eq. (18), we need only to multiply $\ddot{\mathcal{I}}_{jk}^{TT}$ by $(1/c)^2(G/c^2)$. Here, the coordinate positions $x_i = x_i(t)$ refer to the spatial position along the orbit as the particle moves in the effective potential, as a function of time. These expressions for the gravitational waves can be evaluated in our problem by replacing the density function with point particles of the appropriate mass, $\rho(t,\vec{x}) = \sum_\alpha m_\alpha \delta(\vec{x} - \vec{x}_\alpha(t))$.

In practice, the orbital trajectories $\vec{x}_\alpha(t)$ can only be written down in closed form for circular orbits, where the solutions are sinusoids; then, the time derivatives in Eq. (18) can be evaluated analytically. In the case of integrated geodesic trajectories around the black hole considered here, $\vec{x}_\alpha(t)$ will generally be numerical solutions, with derivatives evaluated numerically to give the gravitational waveform.

Gravitational waves are *transverse waves with* two distinct polarization states, defined by the tidal distortion they produce when passing through a region of space. Their effects are commonly envisioned as the time-dependent distortion of the proper distance across a ring of test particles, as shown in Fig. 6. The two polarization states are named "plus" (given by amplitude h_+) and "cross" (given by amplitude $h_\times$) after the principle axes along which the distortions occur.

For circular orbits, the gravitational waveforms are perfect sinusoids, as shown in Fig. 7. As an orbit becomes more eccentric, the gravitational waveforms deviate from sinusoidal shapes, but remain periodic. Examples for orbits with moderate eccentricities are shown in Fig. 8 ($e = 0.9$). The waveforms have the largest amplitudes near periapsis, where the sources are moving most rapidly and the gravitational interactions are strongest (the source is "more relativistic").

An extreme "zoom-whirl" orbit, of the sort EMRIs are expected to have, where the eccentricity is high and the periapsis is near the maximum in the effective potential, is shown in Fig. 9. The amplitude is high and the structure is complex, while the particle is in the whirling phase, moving rapidly in close proximity to the central mass; when the particle zooms out to large distances, the gravitational wave amplitude is comparatively tiny.

V. SIMULATION TOOL

To facilitate exploration of complex gravitational wave sources like EMRIs, we have developed a simulation "dashboard" that allows a user to define a Schwarzschild geodesic orbit of interest by choosing either the orbital parameters, e and r_p, or the effective potential and energy, through the constants of integration, $\tilde{\ell}$ and $\tilde{E}$. The browser-based dashboard is provided as an open-source python package that can be downloaded to run locally (available on

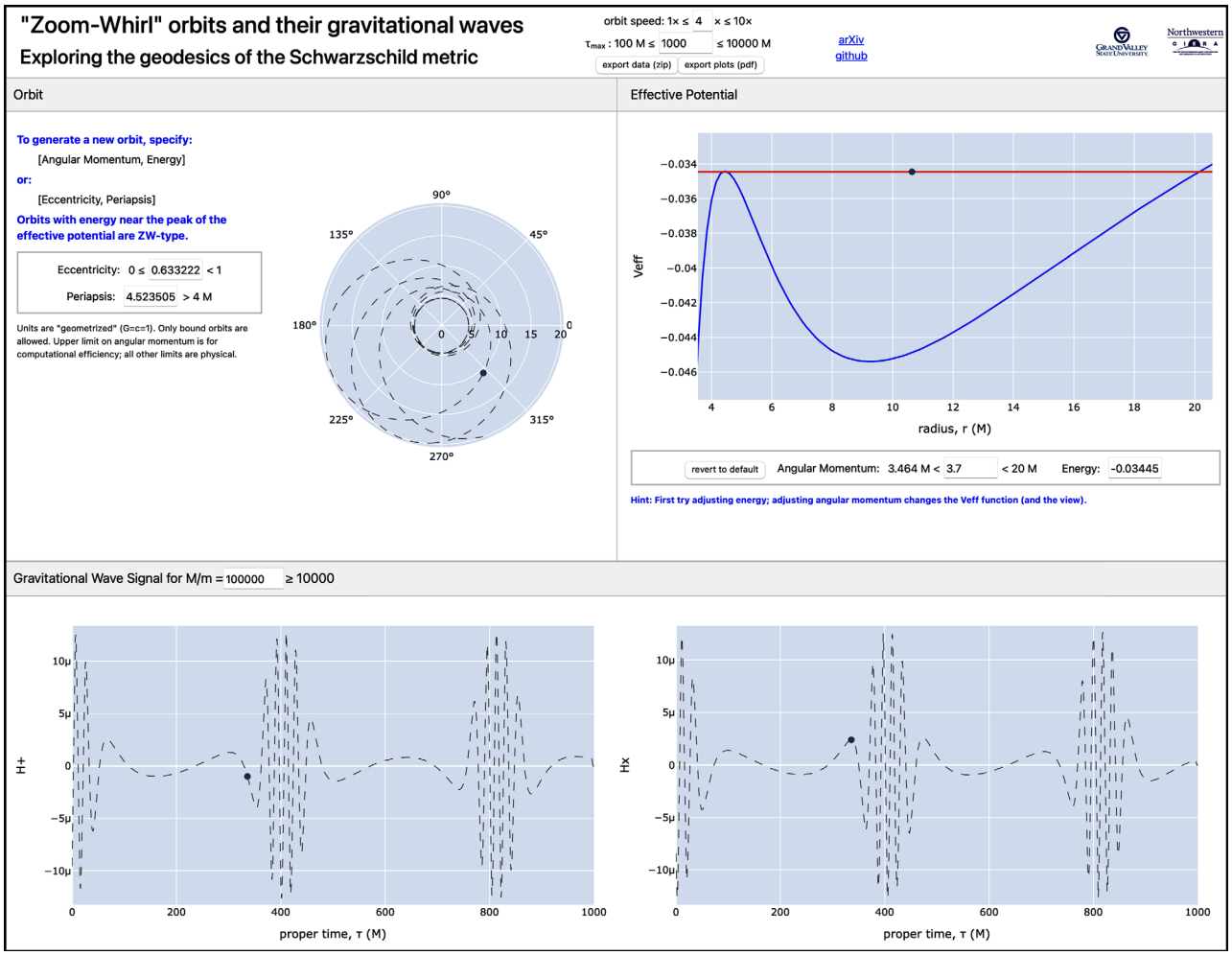

Fig. 10. A screencapture of the online "dashboard"[16] in action, showing the trajectory of a zoom-whirl orbit (upper left), the particle in the effective potential (upper right), and the corresponding gravitational waveforms (lower panels). The update of any parameter by the user immediately changes the simulation; data and figures can be exported for download.

06 December 2024 17:35:28

GitHub[16]), and an online version is linked at ciera.northwestern.edu/gallery/zoom-whirl.

The multi-panel dashboard (Fig. 10) displays a dynamical view of the chosen orbit, including an effective potential graph with the energy of the orbit and the particle's current radial location displayed; a birds-eye view of the orbital trace; and the two gravitational waveform polarizations, $h_+(\tau)$ and $h_\times(\tau)$, as they are produced. By adjusting the orbital parameters, a user can observe in real time how the turning points of the orbits evolve on the potential, and see the impact on both the orbital trajectory and the gravitational waveforms.

VI. DISCUSSION

In this paper, we have outlined how the seemingly exotic "zoom-whirl" behavior of EMRIs can be understood in the context of the effective potential in which the particle moves. In the case of orbits in a Schwarzschild effective potential, conventional circular and elliptical orbits, familiar from Newtonian theory, can be found near the local minimum of the effective potential. However, due to an additional term in the Schwarzschild effective potential, these orbits exhibit the relativistic signature of precession, familiar from Einstein's explanation of the slight "anomalous" perihelion precession of Mercury. For orbits whose inner turning point is very near the local maximum of the effective potential, however, the precession becomes extreme, giving the "whirling" behavior of EMRI orbits. We have provided explicit formulas to calculate the "whirliness" of an orbit, along with representative results.

We have captured these principles in an open-source python-based simulation tool that can either be run locally or online using our publicly accessible version. Pedagogically, it illustrates the utility of effective potentials for understanding orbital motion in a dynamic, interactive way and allows users to explore how traditional elliptical orbits are a part of a continuous family that also includes the "exotic" zoom-whirl orbits from gravitational wave astronomy. The tool shows, in real time, how the effective potential impacts particle motion and gravitational waveforms and also serves as a kind of numerical laboratory for students. We imagine it can be used for demonstration in lecture presentations, but could also be useful as a foundation for exploratory homework problems or laboratory exercises in physics and astronomy courses.

ACKNOWLEDGMENT

B.B. was partially funded by Michigan Space Grant (No. 224029) for this work.

AUTHOR DECLARATIONS

Conflict of Interest

The authors have no conflicts of interest to disclose.

[a]Electronic mail: bolenbr@gvsu.edu
[b]Electronic mail: holderb@gvsu.edu
[c]Electronic mail: s.larson@northwestern.edu

[1]C. A. Manogue, P. J. Siemens, J. Tate, K. Browne, M. L. Niess, and A. J. Wolfer, "Paradigms in physics: A new upper-division curriculum," Am. J. Phys. **69**(9), 978–990 (2001).
[2]C. Cutler, D. Kennefick, and E. Poisson, "Gravitational radiation reaction for bound motion around a Schwarzschild black hole," Phys. Rev. D **50**(6), 3816–3835 (1994).
[3]K. Glampedakis and D. Kennefick, "Zoom and whirl: Eccentric equatorial orbits around spinning black holes and their evolution under gravitational radiation reaction," Phys. Rev. D **66**(4), 044002 (2002).
[4]L. Barack and C. Cutler, "Lisa capture sources: Approximate waveforms, signal-to-noise ratios, and parameter estimation accuracy," Phys. Rev. D **69**(8), 082005 (2004).
[5]R. Haas, "Scalar self-force on eccentric geodesics in Schwarzschild spacetime: A time-domain computation," Phys. Rev. D **75**(12), 124011 (2007).
[6]L. M. Burko and G. Khanna, "Accurate time-domain gravitational waveforms for extreme-mass-ratio binaries," Europhys. Lett. **78**(6), 60005 (2007).
[7]J. Healy, J. Levin, and D. Shoemaker, "Zoom-whirl orbits in black hole binaries," Phys. Rev. Lett. **103**(13), 131101 (2009).
[8]R. Gold and B. Bruegmann, "Eccentric black hole mergers and zoom-whirl behavior from elliptic inspirals to hyperbolic encounters," Phys. Rev. D **88**(6), 064051 (2013).
[9]C.-Q. Liu, C.-K. Ding, and J.-L. Jing, "Periodic orbits around Kerr Sen black holes," Commun. Theor. Phys. **71**(12), 1461–1468 (2019).
[10]LISA collaboration, "Laser Interferometer Space Antenna (LISA) mission concept," Report No. LISA-PRJ-RP-0001 (NASA, 2009).
[11]European Space Agency, "Capturing the ripples of spacetime: LISA gets go-ahead," ESA press release (January 25, 2024), <https://www.esa.int/Science_Exploration/Space_Science/Capturing_the_ripples_of_spacetime_LISA_gets_go-ahead>.
[12]D. Bronicki, A. Cárdenas-Avendaño, and L. C. Stein, "Tidally-induced nonlinear resonances in EMRIS with an analogue model," Class. Quantum Grav. **40**(21), 215015 (2023).
[13]K. S. Thorne, J. A. Wheeler, and C. W. Misner, *Gravitation* (Freeman, San Francisco, CA, 2000).
[14]R. Wald, *General Relativity*, 1st ed. (Chicago U. P., Chicago, IL, 1984).
[15]Precisely, we assume a system of special units (L_s, T_s, M_s) in which $G = 1\,L_s^3\,T_s^{-2}\,M_s^{-1}$ and $c = 1\,L_s\,T_s^{-1}$. An equation can then be nondimensionalized by scaling all physical quantities using the correct combination of the special units—e.g., defining $r' = r/L_s$, $\tilde{V}'_{eff} = \tilde{V}_{eff}/(L_s^2/T_s^2)$, and $M' = M/M_s$—which causes any appearances of c and/or G to cancel out. Thus, all physical quantities in the paper should be thought of as nondimensionalized in this way, but the primed notation will be suppressed.
[16]B. P. Holder and S. Pakiela, see https://github.com/holderbp/zoom-whirl-web-app for "Zoom-Whirl Web App" (2023); Live interactive linked at <https://ciera.northwestern.edu/gallery/zoom-whirl/>.
[17]An English translation of Bertrand's original paper can be found at <https://arxiv.org/abs/0704.2396>.
[18]P. Amaro-Seoane, J. R. Gair, M. Freitag, M. C. Miller, I. Mandel, C. J. Cutler, and S. Babak, "Intermediate and extreme mass-ratio inspirals—Astrophysics, science applications and detection using LISA," Class. Quantum Grav. **24**(17), R113–R169 (2007).
[19]S. Drasco, private communication (2022).
[20]The Schwarzschild solution is a spherically symmetric solution to the Einstein equation. It describes any static, spherically-symmetric, vacuum spacetime. It can represent the space outside a spherical object like a star or planet, or, as we assume here, a static black hole. A full derivation of this equation can be found in any undergraduate relativity text, such those by J. Hartle or T. A. Moore.
[21]B. Schutz, *Gravity from the Ground Up* (Cambridge U. P., Cambridge, UK, 2003).
[22]C. Darwin, "The gravity field of a particle," Proc. R. Soc. London, Ser. A **249**, 180–194 (1959).
[23]C. Darwin, "The gravity field of a particle. II," Proc. R. Soc. London, Ser. A **263**, 39–50 (1961).
[24]E. Poisson and C. M. Will, *Gravity* (Cambridge U. P., Cambridge, UK, 2014).
[25]G. Weinstein, "Einstein's discovery of gravitational waves 1916-1918," arXiv:1602.04040 (2016).
[26]A. Einstein, "Über gravitationswellen," Sitzungsber. Königlich Preuss. Akad. Wiss. **Januar-Juni 1918**, 154–167 (1918).

06 December 2024 17:35:28